Melting Effects of High-Current Relativistic Electron Beam on Aluminum Alloy 1933

A. G. Kobets[a,b], P.R. Horodek[a,c], V. V. Lytvynenko[b], U. F. Lonin[d], A. G. Ponomarev[d], O. A. Startsev[b*], V. T. Uvarov[d]

[a] *Joint Institute of Nuclear Research, 6, Joliot-Curie, str., Dubna,141980, Moscow, Russia*
[b] *Institute of Electrophysics and Radiation Technologies, NAS of Ukraine, Kharkiv, Ukraine 28, Chernyshevsky, str., Kharkiv, 61002, Ukraine*
[c] *Institute of Nuclear Physics, 152, Radzikowskiego, str., Kraków, 31-342, Poland*
[d] *National Science Center Kharkiv Institute of Physics and Technology, NAS of Ukraine, Ukraine 1, Akademicheskaya, str., Kharkov, 61108, Ukraine*
e-mail: startsev-alex@ukr.net

Melting effects of the irradiation by the intense microsecond relativistic hollow electron beam on the wrought aluminum alloy 1933 were studied. The fracture mechanisms for both irradiated and non-irradiated samples and changes in their structure and chemical composition were investigated. The thermal model describing the beam-metal interaction was developed based on the hyperbolic relaxation heat transfer equation, the weakly coupled theory of thermoelasticity, and the Stefan problem. The finite difference method was used to perform calculations according to this model. The areas of modified and non-irradiated material were determined both experimentally and numerically; the quenched, heat-affected and shock-wave-affected zones were localized.

Keywords: aluminum alloy 1933, electron beam, ablation, fracture mechanism.

УДК 621.9.048.7

INTRODUCTION

The effects observed during the interaction of high-current electron beams (HCEB) with metals and alloys are considered to be a good base to develop new radiation nanotechnologies for surface modification through enhancement of physical and mechanical characteristics [1]. The modifying effect is achieved due to a great variety of differently combined processes in the target: fast heating, melting, evaporation, elastic and shock wave formation and propagation, formation and expansion of gas plasma torch, etc. The main feature of e-beam technologies, which distinguishes them from the treatment methods based on the impact of other concentrated energy flows (lasers and plasma), is the maximum of energy deposition, which is released more deeply in the material bulk than others.

Industrial aluminum alloy 1933 of Al-Zn-Mg-Cu system was selected for this study as classified in [2], also considered by us in [3]. Nowadays, it is widely used because of its light density and high durability; typically it operates under cyclic loads [4]. Alloy 1933 has found numerous applications in the aircraft production of An-148, SSJ-100, as well as military aircraft and missile technology, significantly reducing the weight, fuel consumption, increasing the weight efficiency of equipment, its durability, and service life. Alloys of the Al-Zn-Mg-Cu system are wrought alloys that are commonly used in quenched and artificially aged conditions. These high-strength alloys have high vibration resistance and fatigue strength, which favorably differs them from other series of aluminum alloys [2]. On the other hand, these high strength alloys have bad weldability, ductility, malleability; it is also required to improve their crack and corrosion resistance. E-beam processing is one of the possible ways to improve the physical and mechanical properties of alloy 1933. Moreover, to optimize the process of technological HCEB-processing, it is important to study the physical peculiarities of modifying mechanisms in more detail and develop a simple model describing the modification processes.

MATERIALS AND METHODS

The irradiated sample was a square plate of aluminum alloy 1933 (6.35% Zn; 1.6% Mg; 1% Cu; 0.1% Mn; 0.2% Fe; 0.1% Si; 0.06% Ti; 0.05% Cr; 0.1% Zr; 0.0001% Be; the balance Al, % wt.) with thickness ~ 2 mm and side length ~ 10 mm [2, 3]. One-impulse irradiation was conducted under the pressure of about 10^{-5} Tor at the MIG-1 accelerator provided by the NSC Kharkiv Institute of Physics and Technology, with the following parameters: electron energy ~ 0.35 MeV, beam current ~ 2 kA, 5 μs beam pulse in the intensity range up to 10^{12} W/m^2. The pulse duration τ_{imp} was much longer that the electron-phonon relaxation time τ_r (10^{-11} s).

The Gaussian-shaped hollow beam had the inner radius of 15 mm; the outer radius of 23 mm. The energy density released on the surface of the irradiated target was not more than 5 MJ/m^2. The linear dimensions of the plate were larger than the typical size of the interaction region.

Preliminary visual and morphological analysis of the irradiated sample was performed using the optical microscope Bresser BioLux NV. The SEM, fractographic analysis and X-ray microanalysis were conducted using JEOL JSM-840. The Young's modulus, nanohardness were estimated on the polished cross section by Berkovich nanoindentation testing using MSSI's Agilent Nano Indenter G200. We also employed the method of positron annihilation spectroscopy at LEPTA (JINR, Dubna, Russia) [5] to analyze the changes in the defect substructure. To conduct numerical calculations upon the stated below problem, the smoothing coefficients method was used. A numerical model based on the Crank–Nicolson method was implemented in CodeTyphon 4.80, 64-bit Ubuntu 14.04 LTS.

THERMAL MODEL OF E-BEAM ABLATION

In order to describe a physically plausible propagation of the thermal front with a finite velocity, we developed a mathematical model (described by us earlier in [3]) of the evolution of the thermal field in alloy using the relaxation model of the heat flux $\vec{q}$ and the temperature gradient ∇T (1). We use the energy conservation equation (2) and the power of the internal heat source w as defined in Eq.(3). After substitution of (1) into (2) we obtain the hyperbolic heat conduction equation (4):

$$\vec{q}(\vec{r},t) = -\lambda \nabla \mathrm{T}(\vec{r},t) - \tau_r \frac{\partial \vec{q}(\vec{r},t)}{\partial t} - \lambda \tau_r \nabla \frac{\partial T(\vec{r},t)}{\partial t}, \quad (1)$$

$$\frac{\partial T(\vec{r},t)}{\partial t} = -\frac{1}{\rho c} div(\vec{q}) + \frac{w}{\rho c}, \quad (2)$$

$$w(\vec{r},t) = \zeta \int j(\vec{r},t) S(\vec{r},t) d\vec{r} dt, \quad (3)$$

$$\frac{\partial T}{\partial t} + \tau_r \frac{\partial^2 T}{\partial t^2} = \frac{\lambda}{\rho c}\left(\nabla^2 T + \tau_r \nabla^2 \frac{\partial T}{\partial t} \right) + \frac{w}{\rho c} + \frac{\tau_r}{\rho c} \frac{\partial w}{\partial t}, \quad (4)$$

where λ is the coefficient of thermal conductivity, c is the thermal capacity, ρ is the material density, j is the beam current density, S is the energy-deposition profile [3, 6], and the dimensional coefficient $\zeta = 1 \cdot 10^6$ J/(MeV C).

Thereafter, we discretize our problem into two separate parts: finding the temperature field and the thermo-mechanical part. We can apply the weakly coupled dynamic theory of thermoelasticity, taking into account the impact of the deformation rate $\dot{e}$ on the temperature increment $\dot{T}$, if conditions (5) and (6) are fulfilled [3, 7]:

$$\delta_0 = \frac{(3\lambda' + 2\mu')^2 \alpha_T^2 T_0}{c\rho^2 \sqrt{\frac{\lambda' + 2\mu'}{\rho}}} << 1, \quad (5)$$

$$\frac{\dot{e}}{\dot{T}} << \frac{\alpha_T}{\delta_0} \frac{\lambda' + 2\mu'/3}{\lambda' + 2\mu'}, \quad (6)$$

where λ', μ' are the Lame coefficients and α_T is the linear coefficient of thermal expansion. While the energy deposition S has a maximum at a depth of about 120 μm, melting begins earlier within the body than on the surface (we do not consider the sublimation processes). The surface layer irradiated with a dose that is not enough to melt it prevents the evaporation and ejection of the melted material at the mentioned depth under the surface. Therefore, it leads to the formation of the metastable phase in the volume (e.g. superheated liquid melt). The thermo-mechanical part considers the destruction of the aforementioned layer. It happens when the local ultimate strength Ω is equal to a jump of the mechanical tension $|\Xi|$. According to [3, 7], we may simply estimate an upper bound of $|\Xi|$ using its normal-to-surface component σ_{zz}, which defines a tensile jump at the front of the thermoelastic wave (7):

$$|\Xi| \sim \max(\sigma_{zz}) = (3\lambda' + 2\mu')\alpha_T \left(T(z,t) - T_0(z,0) \right). \quad (7)$$

The initial temperature is T_0. The boundary conditions are based on assumptions that the surface temperature at a remote, non-irradiated side is constant and equals T_0 (8), but the incident surface is exposed to the intense irradiation, which results in the multiphase transitions, melting, evaporation, thermal radiation and partial backward condensation of ejected material onto the target (9):

$$T\big|_{z\to\infty} = T_0, \quad (8)$$

$$\lambda \frac{\partial T}{\partial r}\Big|_{z=0} + \beta T\Big|_{z=0} + n^2 \sigma \varepsilon_R T^4\Big|_{z=0} = q_{surf}^{beam} + q^{cond}, \quad (9)$$

where β is the heat transfer coefficient, ε_R is the integral emissivity and n is the refractive index of the environment ($n \approx 1$). q_{surf}^{beam} denotes the heat flux per unit area absorbed by the target (10) and q^{cond} describes the amount of heat released during the backward condensation of ablation products onto the surface (11, 12):

$$q_{surf}^{beam} \approx \zeta \int j(r,t) S(r) dz dt, \quad (10)$$

$$m_{abl} \approx \int \rho dV\Big|_{T>T_{melt}}, \quad (11)$$

$$q^{cond} \approx \theta m_{abl} \left(c(T_{melt} - T_0) + \sum\nolimits_k L_k \right) j(t) e^{-\frac{(t-\varphi)^2}{2D}}, \quad (12)$$

where m_{abl} is the ablated mass, T_{melt} is the melting temperature, θ is the condensation coefficient ($\theta \sim 1/6$), L_k is the latent heat per unit of volume and $D = 1$ s^{-2}, φ is the parameter, which denotes a

delay time of the condensation on the target surface relatively to the beginning of irradiation ($\varphi \sim \tau_{imp}/2$). At moving the boundary of the phase transition, we also set the next conditions (13, 14):

$$T_{j-1}(\xi - 0, t) - T_j(\xi + 0, t) = T_{tran,k}, \quad (13)$$

$$\lambda_{j-1}\frac{\partial T_{j-1}}{\partial r} - \lambda_j \frac{\partial T_j}{\partial r} = L_k \rho \frac{d\xi}{dt}, \quad (14)$$

where ξ is the front of *k*-phase transition that occurs at the transition temperature $T_{tran,k}$.

EXPERIMENTAL AND NUMERICAL RESULTS

Experimental results showed that e-beam irradiation has caused significant erosion to sample and melting of its surface (Fig. 1).The depth of the crater was 0.4 mm at the irradiation epicenter. The sample damage occurred in the combined regime (Fig. 2) with the elements of both the thermal and hydrodynamic regimes [8], which was indicated by the generation of a great amount of a liquid phase as well as of gaseous products. At the beginning of treatment, after the exceeding of a characteristic threshold of the beam power, which defines the transition from the surface desorption to the surface erosion, the ablation of the sample passes in the thermal regime. The ablation products are predominantly gaseous. Further, at high fluxes, there is a certain critical energy density ε* that depends on the shape, duration of the impulse, and the thermophysical parameters of the processing material, then intensive target melting with an explosive behavior in the hydrodynamic regime occurs. The specific damage energy ε_{dam} ($\varepsilon_{dam} = IU\tau_{imp}/m_{abl}$: a ratio of the total effective energy of the incident beam to the mass of ejected material) determines the damage regime. If ε_{dam} is less than the specific energy of melting Q_{melt}, then the damage occurs in the thermal regime, but if ε_{dam} is larger than the specific energy of evaporation is Q_{evap}, then we are dealing with the hydrodynamic regime. Thus, based on these simple calculations, we concluded that the HCEB-modification yielded a combined (or mixed) regime because its specific damage energy was larger than Q_{melt}, but less than Q_{evap}. This mechanism of damage and modification became the main reason of the formation of the unique and complicated structure of the irradiated volume.

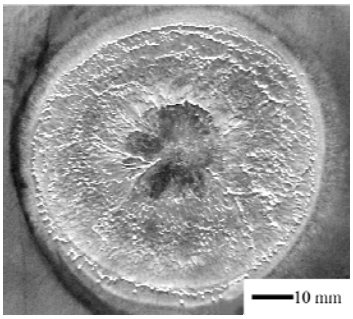

Fig. 1. Surface of aluminum alloy 1933 irradiated by the high-current e-beam.

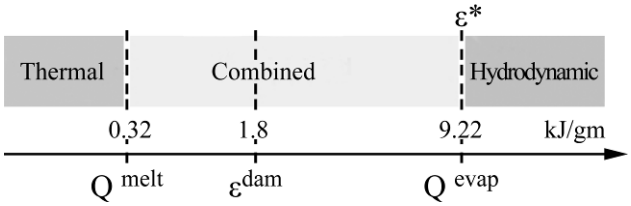

Fig. 2. Comparative scale of energy values corresponding to the fracture mechanisms: thermal, combined and hydrodynamic.

The nature of the sample cross-fractures was investigated (Fig. 3). It was found that the modified volume consists of the quenched zone (QZ), heat-affected (HAZ), and shock-wave-affected zones (SWZ), which differed from each other by their microstructure, chemical composition, fracture mechanisms, concentration, and kinds of defects. However, we have not observed any considerable difference between the HAZ and the SWZ due to the annealing effect of the e-beam processing; thus, we considered those two zones as one. The QZ has a closely packed, fine-grained nonporous structure, which consists of misoriented grains with linear dimensions in the range of 1–3 μm, and its fracture is dimpled and quasi-fibrous (Fig. 3a). The QZ with a thickness of about 200 μm was formed as a result of a high-speed cooling and the backward condensation of ablated material. Both the HAZ and the SWZ with a thickness up to 400 μm were formed due to the influence of the rapid thermal fixation of the shock-wave effect on the melt (Fig. 3b). It is characterized by the micro-ductile fracture mechanism and nonporous fine structure of highly melted facets with a linear size 1 μm without any specific orientation. In contrast, a non-modified alloy (Fig. 3c) is characterized by the well-organized structure of quasi-cleavage crack facets within a size interval of 0.6–1.5 μm. So, the e-beam processing provides a substantial increase of micro-ductile properties.

The results obtained numerically according to the developed thermal model are in good agreement with the experimental data. We calculated the welding penetration depth of such e-beams into the sample: it is not more than 0.8 mm at the irradiation epicenter (peak flux density of up to 10^9 W/sm^2). The microstructure of the modified alloy depends on the heating and cooling rates (R_{ht}, R_{cl}), on the corresponding temperature gradients (G_{ht}, G_{cl}), that, in turn, depend on the heat and mass transfer in the system, which finally influences the alloy composition. The computed heating rate is $R_{ht} \sim 10^8$–10^9 K/s and the heating gradient is $G_{ht} \sim 10^6$–10^8 K/m in the near-surface region (less than 200 μm). The thickness of the quenched layer does not exceed 300 μm in the peripheral regions (flux densities up to 10^6 W/sm^2) and 100–200 μm at the irradiation epicenter, the cooling rate and the temperature gradient $R_{cl} \sim 10^7$–10^8 K/s and $G_{cl} \sim 10^7$–10^8 K/m, respective-

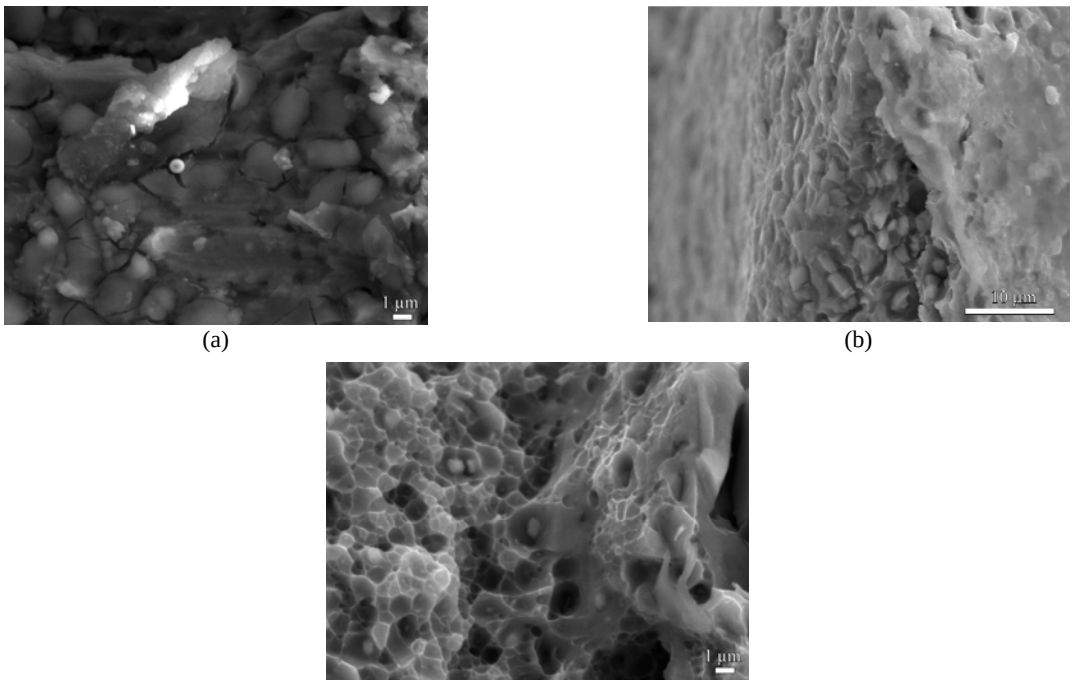

(a) (b)

(c)

Fig. 3. Fractures of sample in: (a) the quenched zone QZ; (b) melted and chock-wave-affected zone HAZ&SWZ; (c) non-irradiated material.

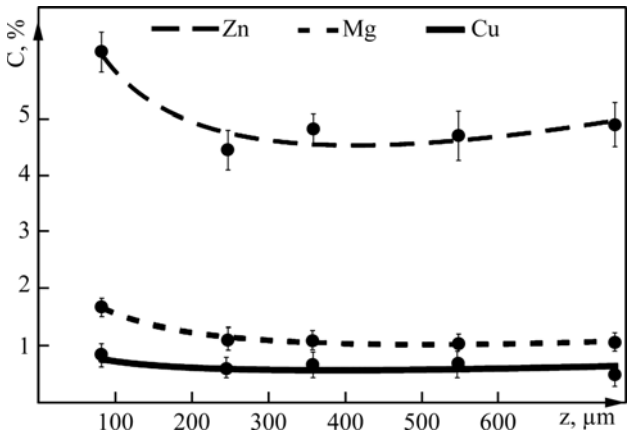

Fig. 4. Chemical composition profile of irradiated sample.

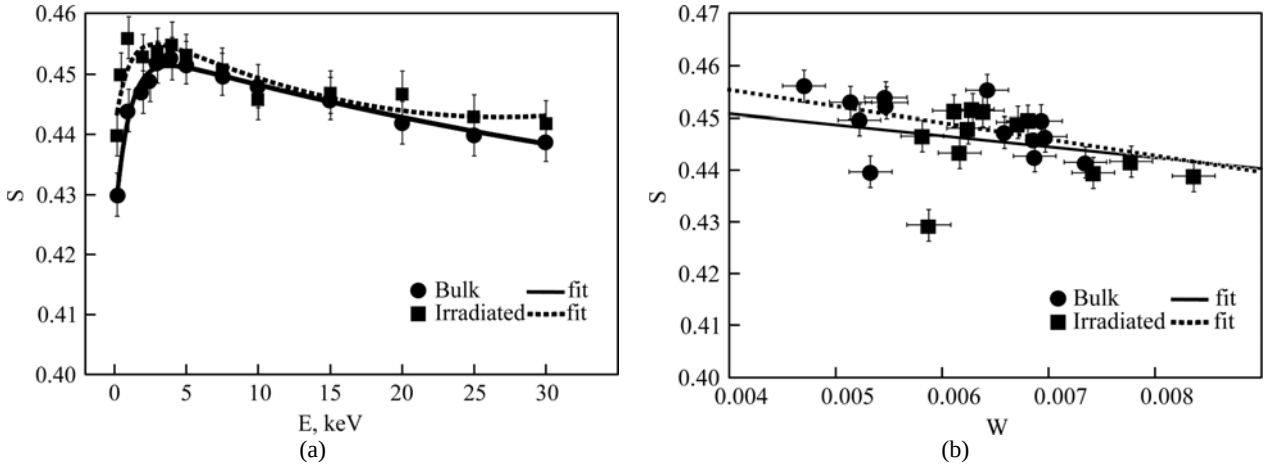

(a) (b)

Fig. 5. Dependences of s-parameter: (a) on *E* positron energy, and (b) on w-parameter, for unmodified bulk and irradiated (in HAZ and SWZ areas) alloy 1933.

ly. The thickness of the melting and of the SWZ is up to 500 μm at the depth of 600–800 μm relatively to the surface, R_{cl} ~ 10^4–10^6 K/s and G_{cl} ~ 10^3–10^5 K/m. Evolution of the ablation interface during the modification process is impulsive due to the inhomogeneous volumetric heat dissipation and localization of stresses. The temperature maximum in the bulk eventually disappears and the crater is broadened. After 2–3 μs, the temperature maximum goes almost to the surface, and the veloci-

ty of the interface between the modified and non-treated material goes into a stationary mode of 100 m/s.

The nanohardness testing revealed an increase in the hardness from 1.5 GPa in the non-modified area to 1.65 GPa, together with an decrease in the Young's modulus from 82 GPa to 79 GPa in the QZ. A decrease in the hardness to 1.36 GPA and an increase in the Young's modulus to 91 GPA were noticed in the HAZ.

Electron probe microanalysis of the sample showed a substantial enrichment (20%) by the major alloying elements Zn, Mg and Cu in the quenched zone at the depth of 120 μm, with the maximal concentrations at the surface (Fig. 4). Probably, this effect occurred due to the diffusion of fusible compounds at the surface. We also conducted the E positron energy (EPA) analysis of our samples (Fig. 5). At the beginning, the Doppler parameter *s* increases linearly with *E* (i.e. with depth, Fig. 5a), describing a presence of the oxide layer on the surface. The large peak in the interval 2–10 keV showed a decline in the degree of crystallinity (little amorphization), which might be caused by the accumulation of any kind of defects, redistribution of alloying elements, or relaxation of high residual stresses near the surface. It should be noted that such a phenomenon could not be caused by the influence of the elastic shock waves, since all investigated volume was formed during the fast crystallization of the melt after irradiation. Recrystallization occurred in the modified volume as evidenced by a small change of *s*-parameter. The e-beam irradiation affected the type of defects towards increasing the number of vacancy defects as indicated by the change in slopes of the straight lines (Fig. 5b).

CONCLUSIONS

The modification of the industrial aluminum alloy 1933 by the high-current electron beam was studied. The e-beam irradiation resulted in a significant enrichment of alloying elements such as Mg, Zn, Cu in the subsurface quenched zone, compared to a non-irradiated sample. The obtained data indicate that the topological behavior of the fracture changes from the quasi-cleavage crack facets to tearing dimples in the unmodified area, to highly melted facets in the transition zone, and to dimpled, dull, quasi-fibrous fracture in the quenched zone. It was proven that e-beam treatment may be efficiently applied to increase the proportion of the micro-ductile fracture in aluminum alloy 1933.

ACKNOWLEDGMENTS

This research was supported by the National Academy of Sciences of Ukraine (grant of the Presidium of NAS of Ukraine № ЦО – 16-2/2014).

REFERENCES

1. Boiko V.I., Valyaev A.N., Pogrebnyak A.D. Metal Modification by High-power Pulsed Particle Beams. *Physics-Uspekhi (Advances in Physical Sciences)*. 1999, **42**(11), 1139–1166.
2. Алюминиевые сплавы : справочник в 6 т. / под ред. И. Н. Фридляндера. М. : Металлургия, 1983–1985.
3. Kobets A.G., Horodek P.R., Lytvynenko V.V., Lonin U.F., Ponomarev A.G, Startsev O.A., Uvarov V.T. Modification of Aluminum Alloy 1933 by the High-Current Electron Beam Irradiation. *Proceedings of the International Conference "Nanomaterials: Applications and Properties", 2014,* **3**(2), 02MAN11(3pp). http://nap.sumdu.edu.ua/index.php/nap/nap2014/paper/view/1535 .
4. Poida V.P., Pedun D.E., Bryukhovetskii V.V., Poida A.V., Sukhov R.V., Samsonik A.L., Litvinenko V.V. Structural Changes during Superplastic Deformation of High-strength Alloy 1933 of the Al–Mg–Zn–Cu–Zr System. *The Physics of Metals and Metallography*. 2013, **114**(9), 779–788.
5. Horodek P., Kobets A., Meshkov I., Pavlov V., Rudakov A., Sidorin A., Yakovenko S. Positron Annihilation Spectroscopy at LEPTA Facility. *Proceeding of the 23rd Russian Particle Accelerator Conference (RuPAC 2012)*. Saint-Petersburg, Russia, 2012, WEPPC044, 532–534.
6. Gann V., den Hartog H., Sugonyako A., Vainshtein D. The Energy Deposition Profile of 0.1-3.0 MeV Electrons in NaCl. *Proceedings of EPAC-2004*. Lucerne, Switzerland, 5–9 July 2004, 2756–2758.
7. Карташов Э.М., Ожерелкова Л.М. Новые модельные представления в проблеме теплового удара. *Математическое моделирование*. 2002, **14**(2), 95–108.
8. Anisimov S.I., Imas Ya.A., Romanov G.S. and Khodyko Yu.V. Action of High-power Radiation on Metals. *Springfield, VA: National Technical Information Service*, 1971, 272 p.

Received 02.09.14

Реферат

Изучены эффекты переплава деформированного алюминиевого сплава 1933 воздействием интенсивным микросекундным релятивистским электронным пучком. Исследованы механизмы разрушения, изменения в структуре и элементном составе облученных и необработанных образцов. Построена тепловая модель описывающая взаимодействие пучка с металлом на основе гиперболического уравнения релаксации теплового потока, слабо связанной теории термоупругости и проблемы Стефана. При проведении численных расчетов согласно разработанной модели использован метод конечных разностей. Экспериментально и численно определены области модифицированного и необлученного материала, локализированы зоны закалки, теплового и ударно-волнового воздействия.

Ключевые слова: алюминиевый сплав 1933, электронный пучок, абляция, механизм разрушения.